

Asymmetric Bimanual Control of Dual-Arm Exoskeletons for Human Cooperative Manipulations

Zhijun Li, Ziting Chen, Arash Ajoudani, Chenguang Yang, Chun-Yi Su, and Antonio Bicchi

Abstract—In this paper, two upper limbs of an exoskeleton robot are operated within a constrained region of the operational space with unidentified intention of human operator’s motion as well as uncertain dynamics including the physical limits. The motion intention of human operator can be modelled as a desired trajectory of his/her limb model of variable force and impedance. Adaptive online estimation for impedance parameters is employed to deal with the nonlinear and variable stiffness property of the limb model. In order for the robot to follow a specific impedance target, we integrate the motion intention estimation into the Barrier Lyapunov Function (BLF) based adaptive impedance control, which can drive the dual-arm exoskeleton tracking target impedance model within the physical ranges of positions and velocities. Experiments have been carried out to test the effectiveness of the proposed dual-arm coordination control scheme, in terms of desired motion and force tracking, as well as human-like natural performance.

I. INTRODUCTION

In the past decades, exoskeleton robots have been developed for human power augmentation, rehabilitation training [1], [2]. One of the most critical issues to control a robotic exoskeleton is to enable the robots understanding the human’s motion intention so that the robots could actively cooperate with the human subject. According to [2], the bimanual tasks for dual-arm manipulation can be classified into two categories: symmetric bimanual task and asymmetric bimanual task and the differences between these two categories are summarised in Table I. Compared with asymmetric tasks for dual-arm manipulation, it is generally easier for a robot to perform symmetric task. However, in practice, most tasks need bimanual dual-arm cooperation in an asymmetric manner, the asymmetric tasks are more popular than symmetric task in practice, and asymmetric tasks bring more challenges in the control design than symmetric tasks. Therefore, in this paper, we develop an asymmetric bimanual coordinate control for a dual-arm exoskeleton system for cooperation with human, in which the left arm implements the constrained motion to a circular object, to which the right arm is attached. The constraint circular object is held by the left hand to follow the trajectory planned in the global frame of coordinate, while the right arm’s end effector follows a trajectory planned on the circular object.

In [3] and [4], the velocities of the two manipulators’ end-effectors can be viewed as relative motions by the introduc-

Z. Li, and Z. Chen are with College of Automation Science and Engineering, South China University of Technology, Guangzhou, China. Email: zjli@ieee.org. C. Yang is with Centre for Robotics and Neural Systems, Plymouth University, UK. Email: cyang@ieee.org. C.-Y. Su is with Department of Mechanical Engineering, Concordia University. Email: cysu@alcor.concordia.

A. Ajoudani, and A. Bicchi are with the Dept. of Advanced Robotics, Istituto Italiano di Tecnologia, Via Morego 30, 16163, Genova, Italy. Arash Ajoudani and A. Bicchi are also with Interdepartmental Research Center “E. Piaggio”, Faculty of Engineering, University of Pisa, Italy. e-mails: arash.ajoudani@iit.it, and bicchi@centropiaggio.unipi.it.

TABLE I

DIFFERENCES BETWEEN SYMMETRIC AND ASYMMETRIC BIMANUAL TASK

Task type	Functions	Motion	Examples
Symmetric	Identical	Identical	Rope climbing
Asymmetric	Different	Different	part assembly, opening bottle.

tion of a relative Jacobian which combines the individual Jacobians of both manipulators together. In [5], by using the relative Jacobian, the kinematic redundancy of dual-arm system was utilized for optimizing torque distributions. In [6], both kinematics and dynamics using relative Jacobian were presented as well, and robust/model-free impedance controller for dual-arm system was proposed. However, the aforementioned works focus on industrial manipulators without consideration of human participation. Moreover, each manipulator is assumed to be redundant and far away from singular configurations. While in practice, singularities and physical constraints can be encountered during performing the task. Therefore, in this paper, we need to consider human cooperation for the robotic exoskeleton, and the position where the singularity happens as the physical constraints of the exoskeleton.

In human robot cooperative manipulation, to enable a robot actively collaborate with the human operator, we must solve the problem that how to make the exoskeleton robot understand the intention of the human operator’s motion. In robotics community, impedance control has been regarded as an effective approach to achieve physical human-robot interaction. When a human subject intends to change the motion, a load force would be produced as the robot extracts its motion in terms of the force exerted by the human subject. To solve this problem, we expect to estimate intention of the operator’s motion, and integrate it into control system design. In this paper, we use the position and force sensors as communication medium between human’ arm and robot’s arm. In order to estimate the motion intention of human operator from available sensory information, much efforts have been made [7], [8] [9]. However, one of main problems of these works is that the variable stiffness property was not considered in the impedance model for motion intention estimation, and consequently the estimation may be not accurate enough.

On the other hand, special consideration should be also taken into the dual-arm exoskeleton with position and velocity constraints in the manipulation tasks for avoiding the singularity region, physical limits and dangerous region, etc. The constraint violation may bring degrade in the control performance. Therefore, it is necessary to carefully deal with the constraints in control design of the various robots [14]. For robot control design, Barrier Lyapunov Functions emerge as a promising approach for handling such physical constraints such as joint limits, torque limits, safety zones [10], [11]. Consider the prob-

lems mentioned above, in this paper we propose an asymmetric bimanual coordinate control for the dual-arm exoskeleton to perform human cooperative manipulation. The contributions can be summarized as follows: (i) the intention of human operator's motion is estimated through impedance parameter identification; and the estimation is embedded into impedance control such that the robot "actively" follow its human subject; (ii) the approach of impedance parameters identification is proposed to estimate the variable stiffness which varies among different subjects, with the instantaneous measurements of force and position of the dual-arm end-effectors, and (iii) a novel BLF-based adaptive impedance control is proposed for the dual-arm exoskeleton under the consideration of the position and velocity constraints.

II. SYSTEM DESCRIPTION

The illustration of asymmetric bimanual manipulation by our dual-arm robot is shown in Fig. 1, where the arm II's end effector tightly holds the circular object moving as required in task space, and the arm I's end effector follows a desired trajectory on the circular object and meanwhile imposes a given certain force on the circular object, where $O_oX_oY_oZ_o$ is the coordinate on the circular object and its origin at the mass centre O_o ; $O_hX_hY_hZ_h$ is the coordinate on the manipulator I's end effector and its origin at the mass centre O_h ; $O_cX_cY_cZ_c$ is the coordinate on the manipulator II's end effector and its origin at the mass centre O_c ; and $OXYZ$ is world coordinate.

The relative position of the system can be described by $\chi_c = \chi_o + A_o(\theta_o)\chi_{co}$, $\chi_h = \chi_o + A_o(\theta_o)\chi_{ho}$, $A_c = A_o(\theta_o)A_{co}(\theta_{co})$, $A_h = A_o(\theta_o)$, where $A_o(\theta_o) \in \mathbb{R}^{3 \times 3}$ represents the rotation matrix of θ_o and $A_{co}(\theta_{co}) \in \mathbb{R}^{3 \times 3}$ denotes the rotation matrix of θ_{co} ; $A_c \in \mathbb{R}^{3 \times 3}$, χ_c , χ_h , and χ_o are the position vectors in $O_cX_cY_cZ_c$, $O_hX_hY_hZ_h$, $O_oX_oY_oZ_o$, respectively, and χ_{co} is the position vector in $O_cX_cY_cZ_c$ expressed in $O_oX_oY_oZ_o$; χ_{ho} is the position vector in $O_hX_hY_hZ_h$ expressed in $O_oX_oY_oZ_o$; θ_c is the orientation vector of $O_cX_cY_cZ_c$; θ_o is the orientation vector of $O_oX_oY_oZ_o$; θ_{co} is the orientation vector of $O_cX_cY_cZ_c$ expressed in $O_oX_oY_oZ_o$; θ_{ho} is the orientation vector of $O_hX_hY_hZ_h$ expressed in $O_oX_oY_oZ_o$; $r_c = [\chi_c^T, \theta_c^T]^T \in \mathbb{R}^6$, $r_h = [\chi_h^T, \theta_h^T]^T \in \mathbb{R}^6$, $r_o = [\chi_o^T, \theta_o^T]^T \in \mathbb{R}^6$, $r_{co} = [\chi_{co}^T, \theta_{co}^T]^T \in \mathbb{R}^6$, $r_{ho} = [\chi_{ho}^T, \theta_{ho}^T]^T \in \mathbb{R}^6$. Considering that the circular object tightly grasped by manipulator II, we have $\dot{r}_{ho} = [\dot{\chi}_{ho}^T, \dot{\theta}_{ho}^T]^T = 0$, accordingly, $\dot{\chi}_{ho} = 0$ and $\dot{\theta}_{ho} = 0$, then we can obtain the derivatives of the relative position as $\dot{\chi}_c = \dot{\chi}_o + A_o(\theta_o)\dot{\chi}_{co} - S(A_o(\theta_o)\chi_{co})\dot{\theta}_o$, $\dot{\chi}_h = \dot{\chi}_o - S(A_o(\theta_o)\chi_{ho})\dot{\theta}_o$, $\dot{\theta}_c = \dot{\theta}_o + A_o(\theta_o)\dot{\theta}_{co}$, $\dot{\theta}_h = \dot{\theta}_o$, where $S(t) = [0, -t_3, t_2; t_3, 0, -t_1; -t_2, t_1, 0]$ [3] with a given vector $t = [t_1, t_2, t_3]^T$. Define $\dot{X}_c = [\dot{\chi}_c^T, \dot{\theta}_c^T]^T$, $\dot{X}_o = [\dot{\chi}_o^T, \dot{\theta}_o^T]^T$, $\dot{X}_h = [\dot{\chi}_h^T, \dot{\theta}_h^T]^T$, $\dot{X}_{co} = [\dot{\chi}_{co}^T, \dot{\theta}_{co}^T]^T$. Then we have the following relationship

$$\dot{X}_{co} = R_A^{-1}\dot{X}_c - R_A^{-1}P\dot{X}_o \quad (1)$$

$$\dot{X}_h = Q\dot{X}_o \quad (2)$$

where $R_A = \text{diag}[A_o(\theta_o), A_o(\theta_o)]$, $P = [I^{3 \times 3}, -S(A_o(\theta_o)\chi_{co}); 0, I^{3 \times 3}]$, $Q = [I^{3 \times 3}, -S(A_o(\theta_o)\chi_{ho}); 0, I^{3 \times 3}]$. Due to the rotation matrix $A_o(\theta_o)$, $A_o(\theta_o)A_o^T(\theta_o) = I^{3 \times 3}$ and $R_AR_A^T = I^{6 \times 6}$, it is

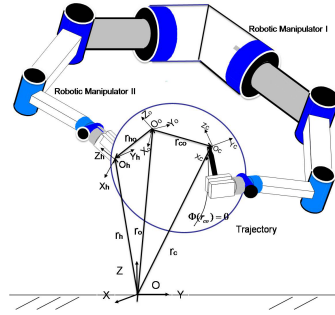


Fig. 1. Schematic diagram of a dual



Fig. 2. The asymmetric bimanual tasks.

obvious that P and Q are of full rank. From (1), one can obtain the relative Jacobian J_R as $\dot{X}_{co} = [R_A^{-1}, -R_A^{-1}P][\dot{X}_c^T, \dot{X}_o^T]^T$. Considering $\dot{X}_c = J_A\dot{q}_A$ and $\dot{X}_o = J_B\dot{q}_B$, and letting $q = [q_A^T, q_B^T]^T$, then we have

$$\begin{aligned} \dot{X}_{co} &= [R_A^{-1}, -R_A^{-1}P][J_A\dot{q}_A, J_B\dot{q}_B]^T \\ &= [R_A^{-1}J_A, -R_A^{-1}PJ_B]\dot{q}^T \end{aligned} \quad (3)$$

where $J_R = [R_A^{-1}J_A, -R_A^{-1}PJ_B]$ is the relative Jacobian in the world coordination.

III. HUMAN-ROBOT COOPERATIVE MOTION GENERATION

Some approaches have been proposed for estimating the stiffness of robot actuators [17]–[20]. However, these approaches can not be applied to human-robot cooperation due to ignoring the human intention estimation. To overcome the practical issue, it is sufficient to consider the case of an additional unknown force function $\varsigma(x, u)$ in [16], i.e.

$$f = m\ddot{x} + b\dot{x} + kx + \varsigma(x, u) \quad (4)$$

where the perfect and complete information of u is not available. Assume that exact values of the applied force f and the position x are measurable, and the corresponding derivatives of these variables can be obtained, and the stiffness-regulating input u is bounded with its first derivative \dot{u} . Then, assume that the ratio between the stiffness regulation rate of change and the velocity of the trajectory measurement is bounded, namely, during the observer application for all times t it holds

$$|\dot{u}(t)| < u|\dot{x}(t)|, \forall t \quad (5)$$

Let $\frac{\partial \varsigma(x, u)}{\partial x} = \xi(x, u)$ denote the stiffness to be measured. Also let $\hat{\xi}(t)$ denote its estimate at time t , and $\tilde{\xi} = \xi(x, u) - \hat{\xi}$ be the estimation error. Differentiate (4) once with respect to time to get

$$\dot{f} = m\ddot{x} + b\dot{x} + kx + \xi\dot{x} + \varsigma_u\dot{u} \quad (6)$$

where $\varsigma_u = \frac{\partial \varsigma(x, u)}{\partial u}$. Using the current estimate of stiffness and the assumptions stated above, a best-effort prediction for \dot{f} can be written (in the absence of information on $\varsigma(x, u)$ and on u) as

$$\dot{\hat{f}} = m\ddot{x} + b\dot{x} + kx + \hat{\xi}\dot{x} \quad (7)$$

The update law can be chosen as

$$\dot{\hat{\xi}} = \alpha \hat{f} \text{sgn}(\dot{x}) \quad (8)$$

with $\alpha > 0$ and $\text{sgn}(\bullet) = \frac{\bullet}{\|\bullet\|}$, if $\|\bullet\| \neq 0$, else, $\text{sgn}(\bullet) = 0$, when $\|\bullet\| = 0$. It is such that $\hat{\xi}$ can be made to converge to the true stiffness value ξ within an uniformly ultimately bounded error.

The traditional mass-damper-spring model to mimic human limb dynamics [16] can be presented as $M_e(\ddot{X}_m - \ddot{X}_e) + B_e(\dot{X}_m - \dot{X}_e) + K_e(X_m - X_e) + \Xi = F_m$, where M_e , B_e and K_e are diagonal matrices and respectively denote the human limb mass, damper and stiffness matrix; Ξ denotes the variable stiffness, $\Xi = [\xi_1, \xi_2, \dots, \xi_n]^T$; X_e represents the human-environment interaction location; F_m is the measured contact force; and X_m is the measurement of Cartesian space coordinate of the dual-arm exoskeleton. In this paper, we view the human limb stiffness as the addition of fixed term K_e and variable term Ξ . From [15], the environment model is mainly related with the damper and spring components, and it can be simplified as

$$B_e(\dot{X}_m - \dot{X}_e) + K_e(X_m - X_e) + \Xi = F_m \quad (9)$$

where B_e and K_e are unknown impedance parameters, and the stiffness K_e can be estimated by the previous method (8). From (9), it is difficult to calculate X_e , even if F_m can be measured by a force sensor, therefore, we need to estimate B_e and K_e .

In human and robot cooperation, human should be active in the task and user inputs control into the system to assist the dual-arm robot to complete the manipulation task, moreover, two arms of the dual-arm exoskeleton robot contact with each other and the interaction force would be produced between them. Two-tiers control loop control is considered in such a manner that the dual-arm exoskeleton robot is controlled to follow the interactive force in between the human limb and the exoskeleton robot. As a result, the interaction force should be minimized. The outer loop generates the human intention trajectory, and the inner loop guarantees position tracking.

Let F_d represent the desired force and $e_f = F_d - F_m$ represent the force tracking-error with the actual force F_m . When the dual arm exoskeleton robot follows human intention, the interaction between robot and its human subject should be small. Therefore, F_d is desired to be equal to 0. The impedance filter is chosen as $G(s) = s/K_f - 1/K_e$ with constant impedance coefficient K_f , and $G(s)E_f(s) = \mathcal{X}_m(s) - \mathcal{X}_r(s) + \Xi(s)/K_e$ is the position perturbation due to the interaction force with $\mathcal{X}_r(s)$, $\mathcal{X}_m(s)$, $\Xi(s)$ and $E_f(s)$ respectively being the Laplace transformations of X_r , X_m , Ξ and e_f . The force tracking error e_f is given by

$$e_f = F_d - F_m = F_d - B_e(\dot{X}_m - \dot{X}_e) - K_e(X_m - X_e) - \Xi \quad (10)$$

$$\mathcal{X}_m(s) = G(s)E_f(s) + \mathcal{X}_r(s) - \Xi(s)/K_e \quad (11)$$

Taking Laplace transformation on (10) and then combining (11), we have

$$E_f(s) = \frac{K_f}{K_e s} [\mathcal{F}_d(s) + B_e s(\mathcal{X}_m(s) - \mathcal{X}_e(s)) - K_e(\mathcal{X}_r(s) - \mathcal{X}_e(s))] \quad (12)$$

where $\mathcal{F}_d(s)$ is the Laplace transformation of F_d . Then the

steady-state force tracking error e_{fs} can be obtained

$$\begin{aligned} e_{fs} &= \lim_{s \rightarrow 0} sE_f(s) \\ &= \lim_{s \rightarrow 0} \frac{K_f}{K_e} (\mathcal{F}_d(s) + K_e \mathcal{X}_e(s) - K_e \mathcal{X}_r(s)) \end{aligned} \quad (13)$$

If the desired position trajectory is precisely selected as,

$$X_r = X_e + F_d/K_e \quad (14)$$

then tracking error of the steady-state force is $e_{fs} = 0$. If the parameters of environment K_e and X_e are accurately known, the reference position trajectory X_r could be generated from (14) to exert the desired interaction force F_d . However, the values of X_e , K_e and B_e are always unknown. Let us consider using its estimate to instead the real values. Here, \hat{F}_m denotes the estimation of F_m , therefore, we have $X_r = \hat{X}_e + \frac{1}{\hat{K}_e} F_d$, where \hat{X}_e and \hat{K}_e are adaptively computed estimates of X_e and K_e , respectively. The measured force F_m from (9) can be written as

$$F_m = K_e X_m + B_e \dot{X}_m - F_0 \quad (15)$$

where $F_0 = K_e X_e + B_e \dot{X}_e - \Xi$, B_e and K_e are the desired values. Considering the estimation of K_e and B_e , we have

$$\hat{F}_m = \hat{K}_e X_m + \hat{B}_e \dot{X}_m - \hat{F}_0 \quad (16)$$

where $\hat{F}_0 = \hat{K}_e \hat{X}_e + \hat{B}_e \dot{\hat{X}}_e - \hat{\Xi}$, \hat{X}_e can be viewed as a predictive of \hat{F}_m , based on the current estimates of \hat{K}_e and \hat{X}_e . From (15) and (16), we can obtain

$$\tilde{F}_m = \tilde{K}_e X_e + \tilde{B}_e \dot{X}_e - \tilde{F}_0 \quad (17)$$

where $\tilde{K}_e = \hat{K}_e - K_e$, $\tilde{B}_e = \hat{B}_e - B_e$, $\tilde{F}_m = \hat{F}_m - F_m$, $\tilde{F}_0 = \hat{F}_0 - F_0$ are estimation errors.

Theorem 3.1: Considering the human limb dynamic model (9), we propose the following adaptation law as

$$\dot{\hat{B}}_{ei} = -\gamma_{Bi} \dot{\chi}_i (\hat{F}_{mi} - F_{mi}) \quad (18)$$

$$\dot{\hat{K}}_{ei} = -\gamma_{Ki} \chi_i (\hat{F}_{mi} - F_{mi}) \quad (19)$$

$$\dot{\hat{X}}_{ri} = \frac{\hat{F}_{mi} - F_{mi}}{\hat{K}_{ei} + \hat{B}_{ei}} [\gamma_{ei} + (\gamma_{Ki} X_{mi} + \gamma_{Bi} \dot{X}_{mi}) \hat{X}_{ri}] \quad (20)$$

$$\dot{\hat{\Xi}}_i = \alpha_i \tilde{F}_{mi} \text{sgn}(\dot{X}_{mi} - \dot{\hat{X}}_{ei}) \quad (21)$$

where α_i , γ_{Bi} and γ_{Ki} are properly selected by the designer, the estimation values \hat{B}_{ei} and \hat{K}_{ei} converge to their respective true values B_{ei} and K_{ei} as $t \rightarrow \infty$, and the corresponding motion generation can be given as

$$X_{ri} = \hat{X}_{ri} + F_{di}/\hat{K}_{ei} \quad (22)$$

$$\hat{K}_{ei}(t) = \hat{K}_{ei}(0) - \gamma_{Ki} \int_0^t X_{mi} (\hat{F}_{mi} - F_{mi}) d\tau \quad (23)$$

$$\hat{B}_{ei}(t) = \hat{B}_{ei}(0) - \gamma_{Bi} \int_0^t \dot{X}_{mi} (\hat{F}_{mi} - F_{mi}) d\tau \quad (24)$$

$$\hat{F}_{mi} = \hat{K}_{ei} (X_{mi} - \hat{X}_{ei}) + \hat{B}_{ei} (\dot{X}_{mi} - \dot{\hat{X}}_{ei}) + \hat{\Xi}_i \quad (25)$$

and the the estimated motion intention is $\hat{X}_{ri}(t) = \hat{X}_{ri}(0) + \int_0^t \frac{\hat{F}_{mi} - F_{mi}}{\hat{K}_{ei} + \hat{B}_{ei}} (\gamma_{ei} + (\gamma_{Ki} X_{mi} + \gamma_{Bi} \dot{X}_{mi}) \hat{X}_{ri}) d\tau$.

Proof: See Appendix. ■

Remark 3.1: According to [21], [22], [23], the human arm parameters are used to discriminate subjects through mapping the suitable control parameters for achieving smooth human-robot interaction. Since a human arm dynamic model can be characterized by its impedance parameters (mass, stiffness and damping), it has been verified that human arm stiffness varied greatly between subjects, tasks, perturbation patterns and experimental devices. A drawing task investigated in the paper requires low velocity, since a high-velocity drawing might not be feasible. During the drawing task, in the impedance characteristic of human arm movements, the range of the stiffness are wider than mass and viscosity. Since both inertia and damping would be decreased in the range of low velocity, the influence of the stiffness parameter is largest among the impedance characteristics, and it dominates the human arm dynamics over the mass and the damping parameters during a human-robot task. Therefore, in the paper, the variation of damping and inertia in the muscle are negligible.

IV. DYNAMICS OF DUAL ARM EXOSKELETON ROBOT

The complete dual-arm exoskeleton dynamics including the human and robot can be described in the joint space as

$$H(q)\ddot{q} + C(q, \dot{q})\dot{q} + M_g(q) + \tau_d = \tau + J_R^T \lambda \quad (26)$$

with $\dot{X}_{co} = J_R \dot{q}$, where q is the dual-arm system's joint variables, and $q = [q_A^T, q_B^T]^T \in \mathbb{R}^n$; q_A is the vector of the manipulator I's joint variables, $q_A \in \mathbb{R}^{n_A}$; q_B is the vector of the manipulator II's joint variables, $q_B \in \mathbb{R}^{n_B}$; n_A is DOF of the manipulator I; n_B is DOF of the manipulator II; n is DOF of the dual-arm exoskeleton robot, and $n = n_A + n_B$; $H(q)$ is the block diagonal of combined inertia matrices, and $H(q) = \text{diag}[M_A(q_A), M_B(q_B)] \in \mathbb{R}^{n \times n}$; $C(q, \dot{q})$ is the combined torques of Coriolis and centrifugal forces, $C(q, \dot{q})q = \text{diag}[C_A^T(q_A, \dot{q}_A)\dot{q}_A, C_B^T(q_B, \dot{q}_B)\dot{q}_B]^T \in \mathbb{R}^n$; $M_A(q_A)$ is the inertial matrix contributed by both the human arm and the exoskeleton manipulator I; $M_B(q_B)$ is the inertial matrix contributed by both human arm and the exoskeleton manipulator II; $C_A(q_A, \dot{q}_A)$ is the Coriolis and centrifugal matrix of the human arm and the exoskeleton manipulator I; $C_B(q_B, \dot{q}_B)$ is the Coriolis and centrifugal matrix of the the human arm and exoskeleton manipulator II; $G_A^T(q_A)$ is the torque of gravitational forces of the human arm and exoskeleton manipulator I; $G_B^T(q_B)$ is the torque of gravitational forces of the human arm and exoskeleton manipulator II; τ is the joint torque vector of dual arms, $\tau = [\tau_A^T, \tau_B^T]^T \in \mathbb{R}^n$ with the control inputs τ_A and τ_B from the manipulator I and II, respectively; τ_h is the human joint torque, $\tau_h \in \mathbb{R}^n$; $M_g(q)$ is the gravitational matrix contributed by both the human operator and exoskeleton robot; τ_d is unknown mechanical disturbance $\tau_d \in \mathbb{R}^n$; $J(q)$ is the Jacobian transformation matrix; $J_R(q)$ is the Jacobian transformation matrix; X is the coordinate in the task space, and $X = [X_o, X_c]^T$; λ is the applied external force, $\lambda \in \mathbb{R}^l$.

Consider an l -dimensional independent constraints in the relative trajectory for the system with a generalized coordinate $q \in \mathbb{R}^n$, which can be expressed as $h(q) = 0 \in \mathbb{R}^l$. The constraint force can be measured by a force sensor on the end-effector and can be converted into joint space as $f = J_R^T(q)\lambda \in$

\mathbb{R}^n where $J_R(q) = \frac{\partial h}{\partial q} \in \mathbb{R}^{l \times n}$, where $\lambda \in \mathbb{R}^l$ is a generalized Lagrangian multiplier.

Inspired by the implicit function theorem in [12], there exists a proper partition of q , i.e., $q = [(q^1)^T, (q^2)^T]^T$ for $q^1 \in \mathbb{R}^{n-l}$, and $q^2 \in \mathbb{R}^l$, where $q^2 = \Omega(q^1)$ with a nonlinear mapping function Ω . Note that the superscript in q^1 and q^2 just denote the index of coordinate partition not the exponent operation. Consider the partition $\dot{X}_{co} = J_R(q)\dot{q}$. It is easy for us to derive $\dot{X}_{co} = [\dot{X}_1^T, \dot{X}_2^T]^T$ and $J_R(q) = \text{diag}[J_1(q), J_2(q)]$, $\dot{X}_1 = J_1 \dot{q}^1$. One can obtain that the terms $\partial \Omega / \partial q^1$ and $\partial^2 \Omega / \partial (q^1)^2$ are bounded. Moreover, we have the following relationship for the independent coordinates q^1, \dot{q}^1 as $q = [(q^1)^T, \Omega(q^1)^T]^T$, $\dot{q} = [I_{n-l}, \frac{\partial \Omega(q^1)}{\partial q^1}]^T \dot{q}^1 = A(q^1)\dot{q}^1$. Differentiating the constraint $h(q) = 0$ with regard to time t , we have $J_R(q)A(q^1)\dot{q}^1 = 0$. Noting that \dot{q}^1 is an independent coordinate, we have $J_R(q)A(q^1) = 0$ and $A^T(q^1)J_R^T(q) = 0$. Due to the velocity transformation, the derivatives of \dot{q} should satisfy $\ddot{q} = A(q^1)\ddot{q}^1 + \dot{A}(q^1)\dot{q}^1$.

To simplify the notations, we will omit variables in function vectors or matrices in the rest of this paper. For example, without causing ambiguity, we will use H, C, M_g, h and A to denote $H(q), C(q, \dot{q}), M_g(q), h(q)$ and $A(q^1)$ respectively. Then, we can have

$$HA\dot{q}^1 + (CA + H\dot{A})\dot{q}^1 + M_g + \tau_d = \tau + J_R^T \lambda \quad (27)$$

Multiplying A^T by both sides of (27), we can obtain

$$\mathcal{H}\dot{q}^1 + \mathcal{C}\dot{q}^1 + \mathcal{G} + \mathcal{T}_d = \mathcal{T} \quad (28)$$

with $\dot{X}_1 = J_1 \dot{q}^1$, where $\mathcal{H} = A^T H A \in \mathbb{R}^{(n-l) \times (n-l)}$, $\mathcal{C} = A^T (CA + H\dot{A}) \in \mathbb{R}^{(n-l) \times (n-l)}$, $\mathcal{G} = A^T M_g \in \mathbb{R}^{n-l}$, $\mathcal{T}_d = A^T \tau_d \in \mathbb{R}^{n-l}$ and $\mathcal{T} = A^T \tau \in \mathbb{R}^{n-l}$.

Property 4.1: The \mathcal{H} and its inverse \mathcal{H}^{-1} are positive and symmetric definite matrices, and the $\mathcal{H} - 2\mathcal{C}$ is a skew-symmetric matrix [13].

V. CONTROL DESIGN

Define error variables $e_1 = X_1 - X_{1d}$, and $e_2 = \dot{q}_1 - \dot{\vartheta}_1$, with a virtual input can be designed as

$$\dot{\vartheta}_1 = J_1^+(q) [-\cos^2(\frac{\pi e_1^T e_1}{2\varepsilon^2}) K_1 e_1 + \dot{X}_{1d}] \quad (29)$$

where ε denotes the constraint on e_1 and can be designed as a small positive constant.

The human joints have physical limits, in order to avoid possible danger to human during the motion, the constraint of tension should be considered in the control design. Therefore, we require errors e_1 and e_2 remain in their respective constraint set $\Omega_1 = \{\|e_1\| < \varepsilon\}$ and $\Omega_2 = \{\|e_2\| < \varrho\}$. It should be noted that due to non-singularity assumption, the pseudo inverse J_1^+ exists, and $J_1 J_1^+ = I$. In order to assure the constraints for X_1 and \dot{q}_1 , we need to guarantee that e_1 and e_2 do not transgress the constrained region.

Consider the following desired control law

$$\mathcal{T}^* = \mathcal{T}_a^* + \mathcal{T}_b^* \quad (30)$$

$$\mathcal{T}_a^* = -\cos^2(\frac{\pi e_2^T \mathcal{H} e_2}{2\varrho^2}) \left(\frac{J_1^T e_1}{\cos^2(\frac{\pi e_1^T e_1}{2\varepsilon^2})} + K_2 e_2 \right) \quad (31)$$

$$\mathcal{T}_b^* = \mathcal{H}\dot{\vartheta}_1 + \mathcal{C}\dot{\vartheta}_1 + \mathcal{G} + \mathcal{T}_d \quad (32)$$

where ϱ denotes the constraint on e_2 and can be designed as a small positive constant, K_2 is a positive definite constant matrix to be designed. Since \mathcal{H} , \mathcal{C} , \mathcal{G} and \mathcal{T}_d can not be obtained beforehand, the designed control law (30) can not be implemented, therefore, we have the following property.

Property 5.1: Define $\Psi = \mathcal{H}\dot{\vartheta}_1 + \mathcal{C}\vartheta_1 + \mathcal{G} + \mathcal{T}_d$, and there exist some unknown finite non-negative constants $c_i \geq 0$ ($i = 1, 2, 3, 4$) such that $\forall q \in R^n$, $\forall \dot{q} \in R^n$, $\|\mathcal{H}\dot{\vartheta}_1\| \leq c_1\|\dot{\vartheta}_1\|$, $\|\mathcal{C}\vartheta_1\| \leq c_2\|\dot{q}\|\|\vartheta_1\|$, $\|\mathcal{G}\| \leq c_3$ and $\|\mathcal{T}_d\| \leq c_4$.

Since $0 \leq \cos^2(\frac{\pi\lambda_{max}e_2^T e_2}{2\varrho^2}) \leq \cos^2(\frac{\pi e_2^T \mathcal{H}e_2}{2\varrho^2}) \leq \cos^2(\frac{\pi\lambda_{min}e_2^T e_2}{2\varrho^2}) \leq 1$, let us define

$$\beta_1 = \cos^2(\frac{\pi\lambda_{max}e_2^T e_2}{2\varrho^2}), \beta_2 = \cos^2(\frac{\pi\lambda_{min}e_2^T e_2}{2\varrho^2}) \quad (33)$$

Definition 5.1: Consider time varying positive function $\delta(t)$ which converge to zero as $t \rightarrow \infty$ and satisfy $\lim_{t \rightarrow \infty} \int_0^t \delta(s)ds = b < \infty$, with finite constant b . Many a choice of $\delta(t)$ satisfy the above condition, for example, $\delta(t) = 1/(1+t)^2$.

To overcome the uncertain dynamics, consider the adaptive robust approach to estimate the unknown entities as

$$\mathcal{T} = \mathcal{T}_a + \mathcal{T}_b \quad (34)$$

$$\mathcal{T}_a = -\frac{\beta_1 J_1^T e_1}{\cos^2(\frac{\pi e_1^T e_1}{2\varepsilon^2})} - \beta_2 K_2 e_2 \quad (35)$$

$$\mathcal{T}_b = -\frac{\beta_2}{\beta_1} \sum_{i=1}^4 \frac{|\hat{c}_i| \Phi_i^2 e_2}{\Phi_i \|e_2\| + \beta_1 \omega_i} \quad (36)$$

where K_2 is a positive definite constant matrix; \hat{c}_i is the estimation of c_i ; ω_i satisfies Definition 5.1, and $\lim_{t \rightarrow \infty} \int_0^t \omega_i(s)ds = b_{1i} < \infty$ with positive constants b_{1i} ($i = 1, 2, 3, 4$); $\Phi = [\|\dot{\vartheta}_1\|, \|\dot{q}\|\|\vartheta_1\|, 1, 1]^T \in \mathbb{R}^6$. As similar to model-based controller (30), \mathcal{T}_a and \mathcal{T}_b can be respectively interpreted as a control input for constraints and a control input that deals with the dynamics of the robot.

Choose the adaptive updating law as $\dot{\hat{c}}_i = -\Gamma_i \left(\sigma_i \hat{c}_i - \frac{\Phi_i^2 \|e_2\|^2}{\beta_1 (\Phi_i \|e_2\| + \beta_1 \omega_i)} \right)$, where Γ_i is a positive constant to be designed; σ_i satisfies Definition 5.1, and $\lim_{t \rightarrow \infty} \int_0^t \sigma_i(s)ds = b_{2i} < \infty$ with positive constants b_{2i} . The stability of the proposed controller (34) is analysed in Appendix.

The designed controller (34) just contains motion control law. For force control, we need design the force controller. Consider (27) and let us derive the force λ as

$$\lambda = Z[(CA + H\dot{A})\dot{q}_1 + M_g + \tau_d - \tau] \quad (37)$$

where $Z = (J_R H^{-1} J_R^T)^{-1} J_R H^{-1}$. Consider the overall control input $\tau = \tau_m + J_R^T \tau_f$ with the motion control τ_m satisfying $\tau_m = A^+ \mathcal{T}$ (A^+ is the left inverse of A^T which can be calculated by $A^+ = A(A^T A)^{-1}$) and the force control τ_f , then one can obtain

$$\lambda = Z[(CA + H\dot{A})\dot{q}_1 + M_g + \tau_d + \tau_h - \tau_m] - \tau_f \quad (38)$$

The force control law is designed as follows

$$\tau_f = \lambda_d - K_f e_\lambda \quad (39)$$

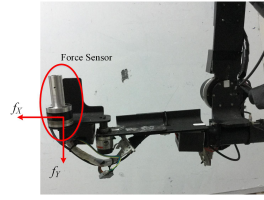


Fig. 3.

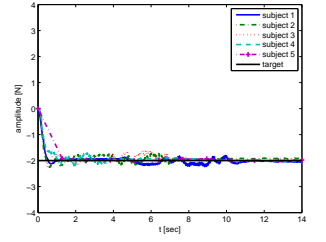


Fig. 4. The external force exerted on the circular object holding by arm II's end effector.

where K_f is a designed parameter, $e_\lambda = \lambda - \lambda_d$. Substituting (39) into (38), we have

$$(K_f + I)e_\lambda = Z[(CA + H\dot{A})\dot{q}_1 + M_g + \tau_d - \tau_m] \quad (40)$$

Theorem 5.1: Consider the dynamics of dual-arm exoskeleton (28) with actuator dynamics, the adaptive controller (34) and the update law \hat{c}_i . If the initial errors satisfy $\|e_1(0)\| < \varepsilon$ and $\|e_2(0)\| < \varrho$, then the following conclusions can be made: (i) all the closed-loop signals are bounded; (ii) for $\forall t > 0$, the constraints $\|e_1(t)\| < \varepsilon$ and $\|e_2(t)\| < \varrho$ hold, where ε and ϱ are two small positive constants to be designed; (iii) the position $X_1(t)$ of the end-effector satisfies $\underline{X}_1(t) < X_1(t) < \bar{X}_1(t)$ with the upper and lower limits $\bar{X}_1(t) = -\varepsilon + X_{1d}(t)$ and $\underline{X}_1(t) = \varepsilon + X_{1d}(t)$, respectively, $\forall t > 0$, which makes the constraints non-violated; (iv) the tracking errors $e_1(t)$ and $e_2(t)$ and $e_\lambda(t)$ converge to the origin, i.e., $X(t) \rightarrow X_{1d}(t)$, $\dot{q}_1(t) \rightarrow \dot{\vartheta}$; (v) the force tracking error e_λ is bounded as $t \rightarrow \infty$.

Proof: See Appendix. ■

VI. EXPERIMENTS

The developed dual arm exoskeleton robot consists of two 5-DOF exoskeleton platforms shown in Fig. 2. There are five revolute joints in the developed exoskeleton. Motors 1, 2, 3, 4 and 5 are the motors for shoulder abduction-adduction, shoulder flexion-extension, elbow flexion-extension, forearm pronation-supination and wrist radial-ulnar deviation, respectively. By using (18) and (19), we can estimate the human intention X_r in (22). Therefore, a force sensor need to be used to measure interactive force between human and the dual-arm exoskeleton robot, as shown in Fig. 3, it is mounted on the end-effector of the right arm.

A drawing task is considered in the experiment shown in Fig. 2. The left arm moves according to the predetermined trajectory on the circular object held by the end effector of the reference right arm. Five joints/DOFs are involved in the experiment, i.e., three joints/DOFs for the left arm to perform drawing task, two joints/DOFs for the right arm to maintain the circular object. The left arm maintains the contact during the drawing. During executing the task, the the desired relative trajectories are designed to keep the end effector of the left arm perpendicular to the surface of the circular object, which is held by the end effector of the right arm. The constant force is exerted in the constrained direction perpendicular on the circular object. We firstly predefine a time-varying target trajectory and secondly

employ the designed human intention estimation method to recognize the human's real intention and then drive the dual-arm exoskeleton robot follow the recognized human intention by the developed adaptive control strategy. Specifically, the shoulder joint of the exoskeleton robot's left arm is constrained between two predefined target positions, i.e., 0.4 rad and 0.0 rad which are respectively depicted by dot dashed line in Fig. 5(a), while the elbow joint of the exoskeleton robot's left arm is expected to be constrained between another two predefined target positions, i.e., 1.6 rad and 0.4 rad which are respectively depicted by dot dashed line in Fig. 5(b). The same experiment are repeatedly performed 5 times with 5 different subjects whose information are Subject 1 (Male, Age:25, Height: 181 cm, Weight: 65kg), Subject 2 (Male, Age: 24, Height: 165 cm, Weight: 59 kg), Subject 3 (Male, Age: 24, Height: 172 cm, Weight: 72 kg), Subject 4 (Female, Age: 28, Height: 158 cm, Weight: 51 kg), and Subject 5 (Female, Age: 23, Height: 160 cm, Weight: 45 kg).

In order to illustrate the advantage of the proposed human intention estimation approach, we also performance a comparison experiment using the conventional impedance control method. It is well known that the impedance model can be described as $M_d(\ddot{X}_m - \ddot{X}_r) + B_d(\dot{X}_m - \dot{X}_r) + K_d(X_m - X_r) = F_m$, where M_d , B_d and K_d are the desired inertia, damping and stiffness matrices, respectively. In the comparative experiment, we choose the impedance parameters as $M_d = \text{diag}[0.0, 0.0]$, $B_d = \text{diag}[7.0, 6.0]$ and $K_d = \text{diag}[0.1, 0.1]$. The controller parameters are chosen as $K_1 = \text{diag}[27.45, 25.8]$, $K_2 = \text{diag}[8.01, 6.4]$, $\varepsilon = 0.03$, $\varrho = 2$, $\lambda_{max} = 3.5336$, $\lambda_{min} = 0.08$, $\omega_j = 5/(t+1)^2$. The force controller parameter in (39) is chosen as $K_f = 5$. The target external force is $\lambda_d = -2.0N$. We choose $\hat{c}_i = 0 (i = 1, 2, 3, 4)$ as the initial values of adaptive laws. Parameters in adaptive laws are set to $\Gamma_i = 0.15$ and $\sigma_i = 2/(t+1)^2$. The interaction force is measured by a force sensor on the end-effector of the right arm. The design parameters with regard to human arm model are chosen as $\gamma_{K_i} = 0.1$, $\gamma_{B_i} = 0.1$ and $\gamma_{e_i} = 0.01$.

The results of experiment on the elbow and shoulder joints are shown in Figs. 5-10. Firstly, the subject 1's experiment results are shown in Fig. 5. The estimated human intention trajectories for the two joints are shown in Figs. 5(a) and 5(b). The two figures illustrate that the positions of these two joints track their respective desired trajectories with small errors. It is obvious that the tracking errors are reducing smaller with time evolves. Fig. 5(c) shows the evolution of the input signals for the corresponding motors. The adaptive parameters are presented in Fig. 5(d). The interaction force is shown in Fig. 5(e). The human arm model parameters, i.e, B_e , K_e and Ξ , are updated in Figs. 5(f)-5(h). From these figures, the desired performance is obtained by using the proposed control scheme, even if little dynamics knowledge of the exoskeleton and the external disturbances in the environment is available. Figs. 5(a) and 5(b) show that the actual position converges to the estimated human intention trajectory. The boundedness of input signals is shown in Fig. 5(c).

For the experiment results of subject 2-5, we only present figures about human intention estimation. Figs. 6-9 show the results of subject 2-5. From these figures, we observe that the

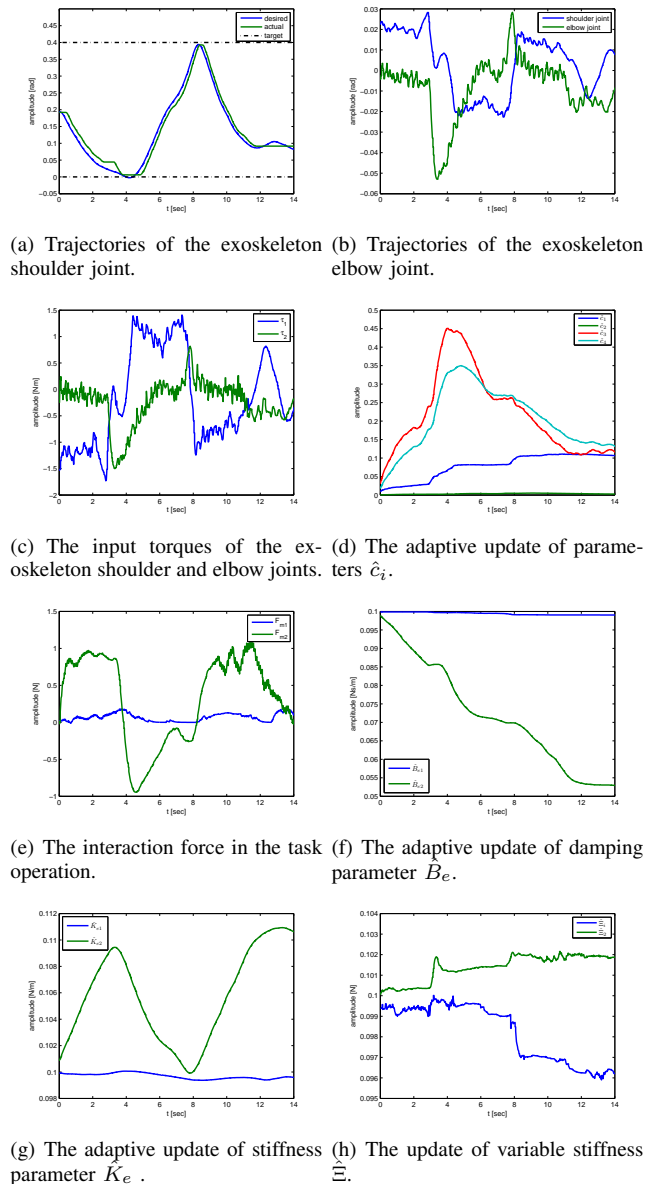
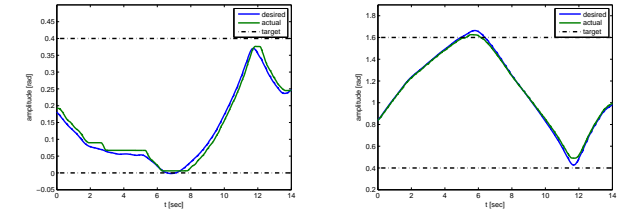


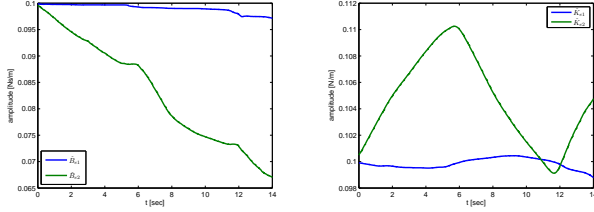
Fig. 5. Experiment results of comparative experiment results for Subject 1.

dual-arm exoskeleton can recognize the human intention by the proposed human intention estimation method and also can track the desired human intention trajectory effectively by the proposed adaptive control strategy. The external force exerted on the circular object holding by arm II's end effector is shown in Fig. 4. We can observe that the actual external force λ tracks the target force λ_d with small tracking error in Fig. 4 for the 5 subject. And the trajectory of λ shows the tendency of converging to the target force λ_d .

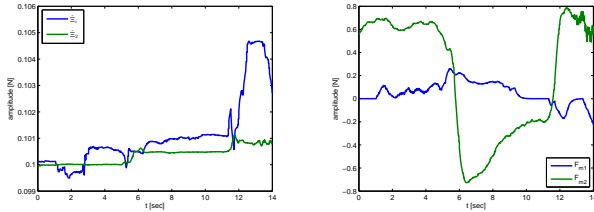
The results of comparative experiment within the 5 subjects using the traditional impedance control method presented in [9] are shown in Fig. 10. The five lines in every figure denote the experiment result of one subject. The estimated human intention for exoskeleton shoulder and elbow joints are presented in Fig. 10(a) and Fig. 10(b). Fig. 10(c) and Fig. 10(d) respectively denotes the measured interaction force in the experiment process. The input torque for the two joints



(a) Trajectories of the exoskeleton shoulder joint. (b) Trajectories of the exoskeleton elbow joint.

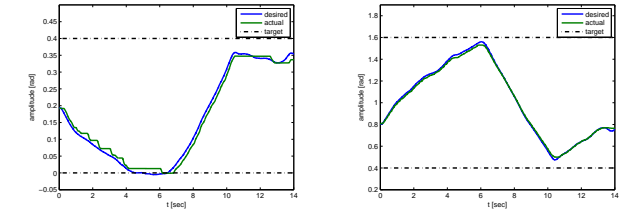


(c) The adaptive update of damping parameter \hat{B}_e . (d) The adaptive update of stiffness parameter \hat{K}_e .

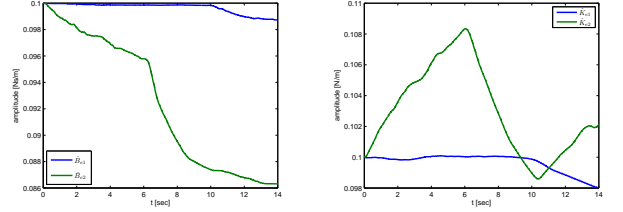


(e) The update of variable stiffness $\hat{\Xi}$. (f) The interaction force in the task operation.

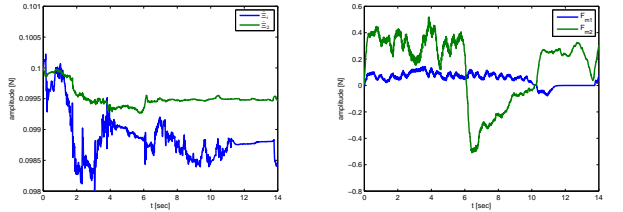
Fig. 6. Experiment results of subject 2.



(a) Trajectories of the exoskeleton shoulder joint. (b) Trajectories of the exoskeleton elbow joint.



(c) The adaptive update of damping parameter \hat{B}_e . (d) The adaptive update of stiffness parameter \hat{K}_e .



(e) The update of variable stiffness $\hat{\Xi}$. (f) The interaction force in the task operation.

Fig. 7. Experiment results of subject 3.

are shown in Fig. 10(e) and Fig. 10(f). From the subplot (f) of Figs. 5-9 and Fig. 10(c) and Fig. 10(d), we can observe that when using our human intention identification scheme, the interactive force between exoskeleton robot arm and its human partner is smaller. In the comparative experiment, we use same impedance parameters for the 5 subjects. Moreover, we have compared the inter-subject experiment results in Figs. 5-9. From these figures, we can see that the estimated human arm parameters B_e , K_e and Ξ are considerable different. It is understandable because different human should have different arm parameters. The developed method can identify its human partner's arm parameters and then use the recognized parameter synthesizing the desired human intention that the exoskeleton robot to precisely follow.

VII. CONCLUSION

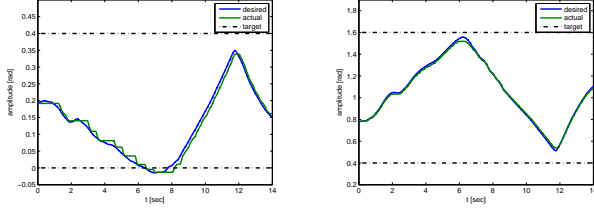
The paper developed a Barrier Lyapunov Function (BLF) based adaptive impedance control for dual-arm exoskeleton with unknown intention of the human operator, unknown robot dynamics, and the physical limits. Motion intention of human operator is considered as the desired trajectory and impedance parameter online identification is employed to deal with the nonlinear and variable stiffness property of human limb model. Experiments have been conducted to demonstrate that the proposed dual-arm coordination controller is effective. In the future work, we shall consider stroke patients participated in the actual experiments.

APPENDIX

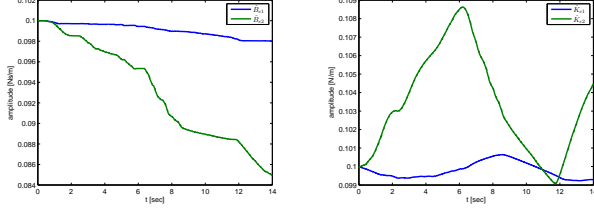
Consider the Barrier Composite Energy Function candidate as $V = \frac{\varepsilon^2}{\pi} \tan(\frac{\pi e_1^T e_1}{2\varepsilon^2}) + \frac{\varrho^2}{\pi} \tan(\frac{\pi e_2^T \mathcal{H}e_2}{2\varrho^2}) + \frac{1}{2} \sum_{i=1}^4 \frac{1}{\Gamma_i} \tilde{c}_i \dot{\tilde{c}}_i + \sum_{i=1}^n \frac{1}{2\gamma_{B_i}} \hat{B}_{ei}^2 + \sum_{i=1}^n \frac{1}{2\gamma_{K_i}} \hat{K}_{ei}^2 + \sum_{i=1}^n \frac{1}{2\gamma_{F_i}} \hat{F}_{0i}^2$, where $\tilde{c}_i = \hat{c}_i - c_i$. Considering the derivative of V and using Property 4.1 and (18) and (19), by defining $\hat{F}_{0i} = \gamma_e(\hat{F}_{mi} - F_{mi})$ we have

$$\begin{aligned} \dot{V} \leq & -e_1^T K_1 e_1 + \frac{e_1^T J_1 e_2}{\cos^2(\frac{\pi e_1^T e_1}{2\varepsilon^2})} - \frac{e_2^T}{\cos^2(\frac{\pi e_2^T \mathcal{H}e_2}{2\varrho^2})} (\mathcal{C}\vartheta_1 \\ & + \mathcal{G} + \mathcal{T}_d + \mathcal{H}\vartheta_1) + \frac{e_2^T \mathcal{T}}{\cos^2(\frac{\pi e_2^T \mathcal{H}e_2}{2\varrho^2})} + \sum_{i=1}^4 \frac{1}{\Gamma_i} \tilde{c}_i \dot{\tilde{c}}_i \end{aligned} \quad (41)$$

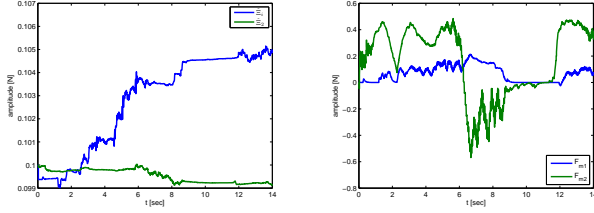
Integrating (34) into (41), considering (33) and Property 5.1, and using the fact of $-\beta_2/\cos^2(\frac{\pi e_2^T \mathcal{H}e_2}{2\varrho^2}) \leq -1$, we can rewrite \dot{V} as $\dot{V} \leq -e_1^T \left(K_1 - \alpha/2 \cos^2(\frac{\pi e_1^T e_1}{2\varepsilon^2}) \right) e_1 - e_2^T \left(K_2 - \alpha/2 \cos^2(\frac{\pi e_1^T e_1}{2\varepsilon^2}) \right) e_2 + \frac{e_2^T \mathcal{T}_b - e_2^T \Psi}{\cos^2(\frac{\pi e_2^T \mathcal{H}e_2}{2\varrho^2})}$, where $\alpha = \|\mathcal{J}_1\| (1 - \frac{\beta_1}{\beta_2})$. Considering the following inequality, which is bounded by $\frac{e_2^T \mathcal{T}_b}{\cos^2(\frac{\pi e_2^T \mathcal{H}e_2}{2\varrho^2})} - \frac{e_2^T \Psi}{\cos^2(\frac{\pi e_2^T \mathcal{H}e_2}{2\varrho^2})} + \frac{1}{2} \sum_{i=1}^4 \Gamma_i^{-1} \tilde{c}_i \dot{\tilde{c}}_i \leq \sum_{i=1}^4 c_i \omega_i - \sum_{i=1}^4 \frac{1}{2} \sigma_i \tilde{c}_i \dot{\tilde{c}}_i + \sum_{i=1}^4 \frac{1}{2} \sigma_i c_i^2$, where we use the facts: $-\beta_2/\cos^2(\frac{\pi e_2^T \mathcal{H}e_2}{2\varrho^2}) \leq -1$, $\frac{\beta_1 c_i \Phi_i \|e_2\| \omega_i}{\Phi_i \|e_2\| + \beta_1 \omega_i} \leq \beta_1 c_i \omega_i$ and $-\dot{\tilde{c}}_i \leq -\hat{c}_i (i = 1, \dots, 4)$. The last inequality obtained is



(a) Trajectories of the exoskeleton shoulder joint. (b) Trajectories of the exoskeleton elbow joint.

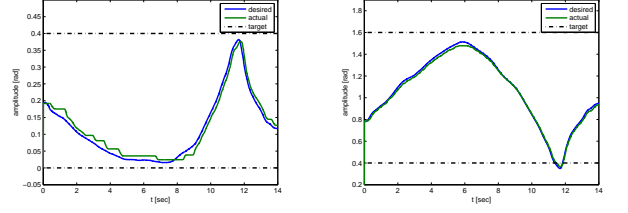


(c) The adaptive update of damping parameter \hat{B}_e . (d) The adaptive update of stiffness parameter \hat{K}_e .

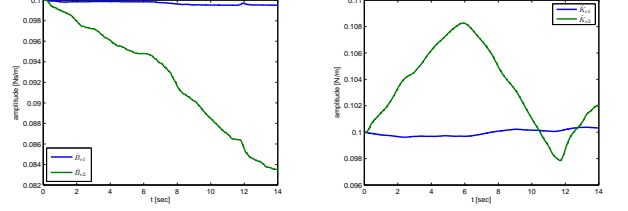


(e) The update of variable stiffness parameter $\hat{\sigma}$. (f) The interaction force in the task operation.

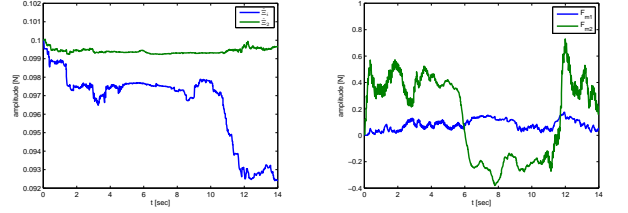
Fig. 8. Experiment results of subject 4.



(a) Trajectories of the exoskeleton shoulder joint. (b) Trajectories of the exoskeleton elbow joint.



(c) The adaptive update of damping parameter \hat{B}_e . (d) The adaptive update of stiffness parameter \hat{K}_e .



(e) The update of variable stiffness parameter $\hat{\sigma}$. (f) The interaction force in the task operation.

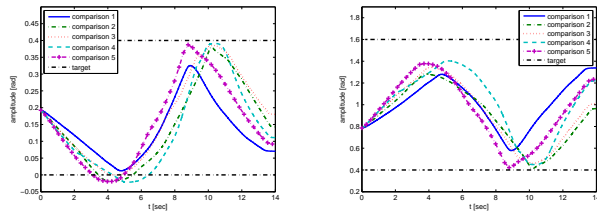
Fig. 9. Experiment results of subject 5.

because that $-\tilde{c}_i \hat{c}_i = -\tilde{c}_i(c_i + \tilde{c}_i) = -\tilde{c}_i \tilde{c}_i - \tilde{c}_i c_i$ and $-\tilde{c}_i c_i \leq \frac{1}{2}(\tilde{c}_i \tilde{c}_i + c_i c_i)$, we have $-\tilde{c}_i \hat{c}_i \leq -\frac{1}{2}\tilde{c}_i \tilde{c}_i + \frac{1}{2}c_i c_i$. Then, we can rewrite \dot{V} as $\dot{V} \leq -e_1^T \left(K_1 - \alpha/2 \cos^2(\frac{\pi e_1^T e_1}{2\varepsilon^2}) \right) e_1 - e_2^T \left(K_2 - \alpha/2 \cos^2(\frac{\pi e_2^T e_2}{2\varepsilon^2}) \right) e_2 + \sum_{i=1}^4 c_i \omega_i + \sum_{i=1}^4 \frac{1}{2} \sigma_i c_i^2 - \sum_{i=1}^4 \frac{1}{2} \sigma_i \tilde{c}_i \tilde{c}_i$. Since $\sum_{i=1}^4 c_i \omega_i \rightarrow 0$ and $\sum_{i=1}^4 \frac{1}{2} \sigma_i c_i^2 \rightarrow 0$ as $t \rightarrow \infty$ due to the definition of ω_i and σ_i , and by selecting the suitable positive definite constant matrices K_1 , K_2 satisfying $K_1 \geq \frac{\alpha}{2} I$ and $K_2 \geq \frac{\alpha}{2} I$, and positive constants $\Gamma_i (i = 1, \dots, 4)$, one can conclude that $\dot{V} < 0$ as $t \rightarrow \infty$. Thus, e_1 and e_2 converge to the origin as $t \rightarrow \infty$. Integrating both sides of the above equation gives $V(t) - V(0) \leq -\int_0^t \left\{ e_1^T \left(K_1 - \alpha/2 \cos^2(\frac{\pi e_1^T e_1}{2\varepsilon^2}) \right) e_1 + e_2^T \left(K_2 - \alpha/2 \cos^2(\frac{\pi e_2^T e_2}{2\varepsilon^2}) \right) e_2 + \sum_{j=1}^4 \frac{1}{2} \sigma_j \tilde{c}_j \tilde{c}_j \right\} ds + \int_0^t \left\{ \sum_{i=1}^4 c_i \omega_i + \sum_{i=1}^4 \frac{1}{2} \sigma_i c_i^2 \right\} ds$. Since c_i is constant $\int_0^\infty \omega_i ds = b_{1i}$ and $\int_0^\infty \sigma_i ds = b_{2i} (i = 1, \dots, 4)$ are constants, we can rewrite it as $V(t) - V(0) < \infty$. Thus, V is bounded such that $e_1, e_2 \in L_\infty$ and $X \in L_\infty$ according to the boundedness of X_{1d} in Assumption 3.1. We can conclude that J_1 and q are bounded. Since c_i is a constant, we have \hat{c}_i is also bounded. Then, we can obtain the follows. (i) Since the augmented Lyapunov function V is bounded, it is obvious that all the closed-loop signals are

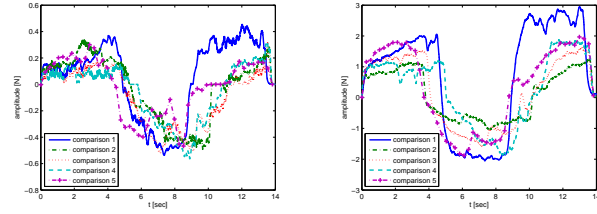
all bounded. (ii) Assume that there exists some $t = T$ such that $\|e_1(t)\|$ or $\|e_2(t)\|$ grows to their respective constraint ε or ϱ , i.e., $\|e_1(T)\| = \varepsilon$ or $\|e_2(T)\| = \varrho$. The initial values $\|e_1(0)\| < \varepsilon$ and $\|e_2(0)\| < \varrho$. Then, it is obtained that V rises infinite by substituting $e_1(T)$ or $e_2(T)$ into \dot{V} . However, V is bounded. According to the method of proof by contradiction, we have the constraints $\|e_1(t)\| < \varepsilon$ and $\|e_2(t)\| < \varrho$ holding for $\forall t > 0$. (iii) We have $\|e_1(t)\| < \varepsilon$ from (ii). From the definition of $e_1(t)$, we have $X_1(t) = e_1(t) + X_{1d}(t)$. Then, it obtains $-\varepsilon + X_{1d}(t) < X_1(t) < \varepsilon + X_{1d}(t)$, which indicates $\underline{X}_1(t) < X_1(t) < \bar{X}_1(t)$ where $\bar{X}_1(t) = -\varepsilon + X_{1d}(t)$ and $\underline{X}_1(t) = \varepsilon + X_{1d}(t)$. (iv) According to the Definition 5.1, we have $\omega_j \rightarrow 0$ and $\sigma_j \rightarrow 0 (j = 1, \dots, 4)$ as $t \rightarrow \infty$. We have $\dot{V} \leq 0$ as $t \rightarrow \infty$ by choosing appropriate design parameters K_1, K_2 and $\Gamma_j (j = 1, \dots, 4)$, $X(t) \rightarrow X_{1d}(t)$ and $\hat{q}_1(t) \rightarrow \vartheta$. (v) Since $e_2 = \hat{q}_1 - \vartheta_1$ and ϑ_1 are bounded, \hat{q}_1 is also bounded. Then $Z, C, A, \hat{A}, M_g, \tau_h$ and τ_m in (40) are both bounded. Considering the bounded H and \hat{q}_1 , we obtain the right hand side of (40) is bounded. In other words, $(K_f + I)e_\lambda$ is bounded. Then the force error e_f is bounded.

REFERENCES

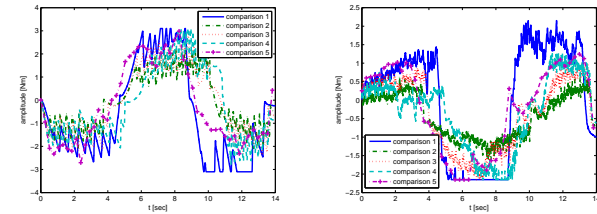
- [1] J. Ueda, D. Ming, V. Krishnamoorthy, M. Shinohara, and T. Ogasawara, "Individual muscle control using an exoskeleton robot for muscle function testing", *IEEE Trans. Neural Systems and Rehabilitation Engineering*, vol. 18, no. 4, Aug. 2010, pp. 339-350.



(a) Trajectories of the exoskeleton shoulder joint. (b) Trajectories of the exoskeleton elbow joint.



(c) The interaction force F_{m1} . (d) The interaction force F_{m2} .



(e) The input torque of the exoskeleton shoulder joints. (f) The input torque of the exoskeleton elbow joints.

Fig. 10. Comparative experiment results of the 5 subjects.

[2] M. Trlep, M. Mihelj, and M. Munih, "Skill transfer from symmetric and asymmetric bimanual training using a robotic system to single limb performance," *Journal of NeuroEngineering and Rehabilitation*, vol. 9, no. 43, 2012, pp. 1-14.

[3] Z. Li, P. Tao, S. S. Ge, M. D. Adams, W. S. Wijesoma, "Robust adaptive control of cooperating mobile manipulators with relative motion," *IEEE Trans. System, Man, and Cybernetics, Part B*, vol. 39, no. 1, 2009, pp. 103-116.

[4] Z. Li, S. Deng, C.-Y. Su, G. Li, Z. Yu, Y. Liu, M. Wang, "Decentralized adaptive control of cooperating mobile manipulators with disturbance observers," *IET Control Theory & Application*, vol. 8, no. 7, May, 2014, pp.515-521.

[5] W. S. Owen, E. A. Croft, B. Benhabib, "Acceleration and torque redistribution for a dual-manipulator system," *IEEE Transactions on Robotics*, vol.21, no.6, Dec. 2005, pp. 1226-1230.

[6] J. Lee, P. H. Chang and R. S. Jamisola, "Relative impedance control for dual-arm robots performing asymmetric bimanual tasks," *IEEE Transactions on Industrial Electronics*, vol.61, no.7, July 2014, pp.3786-3796.

[7] R. Riemer, L. Lunenburger, S. Jezernik, M. Anderschitz, G. Colombo, and V. Dietz, "Patient-Cooperative Strategies for Robot-Aided Treadmill Training: First Experimental Results," *IEEE Trans. Neural Systems and Rehabilitation Engineering*, vol. 13, no. 3, pp. 380-394, Sep. 2005.

[8] K. Wakita, J. Huang, P. Di,K. Sekiyama, and T. Fukuda, "Human-walkingintention- based motion control of an omnidirectional-type cane robot," *IEEE/ASME Trans. Mechatronics*, vol. 18, no. 1, pp. 285-296, Feb. 2013.

[9] Y. Li and S. S. Ge, "Human-Robot Collaboration Based on Motion Intention Estimation," *IEEE/ASME Transactions on Mechatronics*, vol. 19, no. 3, 2014, pp. 1007-1014.

[10] K. P. Tee, S. S. Ge, E. H. Tay, "Barrier Lyapunov Functions for the control of output-constrained nonlinear systems," *Automatica*, vol. 45, no. 4, Apr. 2009, pp. 918-927.

[11] K. P. Tee, B. Ren, and S. S. Ge, "Control of nonlinear systems with time-varying output constraints," *Automatica*, vol. 47, no. 11, Nov. 2011, pp. 2511-2516.

[12] N. H. McClamroch and D. Wang, "Feedback stabilization and tracking

of constrained robots," *IEEE Transactions on Automatic Control*, vol. 33, no. 5, May 1988, pp. 419-426.

[13] Z. Li, S. S. Ge, *Fundamentals in modeling and control of mobile manipulators*, CRC Press, May 2013.

[14] W. He, S. Zhang, and S. S. Ge, "Adaptive control of a flexible crane system with the boundary output constraint," *IEEE Trans. Industrial Electronics*, vol. 61, no. 8, Aug. 2014, pp. 4126-4133.

[15] D. Erickson, M. Weber, I. Sharf, "Contact stiffness and damping estimation for robotic systems," *The International Journal of Robotics Research*, vol. 22, no. 1, 2003, pp. 41-57.

[16] M. Rahman, R. Ikeura, and K. Mizutani, "Investigation of the impedance characteristic of human arm for development of robots to cooperate with humans," *JSME Int. J. Series C*, vol. 45, no. 2, pp. 510-518, 2002.

[17] G. Brioli, A. Bicchi, "A Non-Invasive, Real-Time Method for Measuring Variable Stiffness," in *Proc. Robotics Science and Systems (RSS 2010)*, Zaragoza, 2010.

[18] F. Flacco, A. De Luca, I. Sardellitti, N. G Tsagarakis, "On-line estimation of variable stiffness in flexible robot joints," *International Journal of Robotics Research*, vol. 31, no. 13 1556-1577, Nov. 2012.

[19] T. Menard, G. Grioli, A. Bicchi, "A real time robust observer for an agonist-antagonist variable stiffness actuator," In *International Conference on Robotics and Automation*, 2013, pp. 3988-3993.

[20] G. Grioli, A. Bicchi, "A real-time parametric stiffness observer for VSA devices," In *International Conference on Robotics and Automation*, 2011, pp. 5535-5540.

[21] D. E. Barkana, N. Sarkar, "Towards a smooth humanCrobot interaction for rehabilitation robotic systems," *Advanced Robotics*, vol. 23, nos. 12-13, pp. 1641-1662.

[22] C. Mitsantisuk, S. Katsura, and K. Ohishi, "Kalman-filter-based sensor integration of variable power assist control based on human stiffness estimation," *IEEE Trans. Industrial Electronics*, vol. 56, no. 10, Oct. 2009, pp. 3897-3905.

[23] T. Tsumugiwa, R. Yologawa, and K. Ham, "Variable impedance control based on estimation of human arm stiffness for human-robot cooperative calligraphic task," *Proceedings of the 2002 IEEE International Conference on Robotics Automation*, 2002, pp. 644-649.